Available online at www.sciencedirect.com
ScienceDirect
Applied Thermal Engineering 28 (2008) 1047–1057
APPLIED THERMAL ENGINEERING
www.elsevier.com/locate/apthermeng

Transient cooling of electronics using phase change material (PCM)-based heat sinks

Ravi Kandasamy, Xiang-Qi Wang, Arun S. Mujumdar *

Engineering Science Program and Department of Mechanical Engineering, National University of Singapore, 10 Kent Ridge Crescent, Singapore 119260, Singapore

Received 23 December 2006; accepted 19 June 2007
Available online 24 June 2007

Abstract

Use of a phase change material (PCM)-based heat sink in transient thermal management of plastic quad flat package (QFP) electronic devices was investigated experimentally and numerically. Results show that increased power inputs enhance the melting rate as well as the thermal performance of the PCM-based heat sinks until the PCM is fully melted. A three-dimensional computational fluid dynamics model was proposed to simulate the problem and demonstrated good agreement with experimental data. Results indicate the potential for PCM-based heat sinks for use in intermittent-use devices.

Keywords: Phase change materials; Heat sink; Electronics cooling; Thermal management

1. Introduction

Technological enhancements at the device, package and system levels have resulted in increased functionality and decreased form factors, but squeezed more power into ever-small packages. As a consequence, thermal management has become more critical for successful design of electronic devices such as cellular phones, digital cameras, notebooks and personal digital assistants (PDA), etc. Such devices are not operated continuously over long periods, so a phase change material (PCM)-based cooling system has potential for application. Integrated circuits operate best within a limited temperature range; hence their packages must be designed to remove the excessive heat. As an alternative passive cooling technique means, PCMs have been widely investigated for such transient electronic cooling applications considering their advantages such as high latent heat of fusion, high specific heat, controllable temperature stability and small volume change during phase change, etc.

Gong and Mujumdar [1–4] have carried out a series of numerical studies on heat transfer during melting and freezing of single and multiple PCMs. A new design for thermal storage using multiple PCMs was first proposed by them for power generation in space-based activities [1]. They extended their analysis from only the charge process (melting) to a combined charge/discharge (melting/freezing) process [2]. In [4], by a thermodynamic analysis, Gong and Mujumdar found that the increase of the overall thermal efficiency could theoretically be doubled, or even tripled by use of multiple PCMs. Kandasamy et al. [5] experimentally and numerically studied various parameters for a novel PCM package for thermal management of portable electronic devices, such as power input, orientation of package and various melting/freezing times under cyclic steady conditions.

The low thermal conductivity of most PCMs presents a significant challenge in the design of PCM-based electronic cooling systems. In order to overcome this drawback, researchers have proposed various heat transfer enhancement techniques, e.g., use of partitions/fins, graphite/metal matrices, dispersed high-conductivity particles in the PCM, multiple PCMs [6] and micro-encapsulation of PCM [7,8].

* Corresponding author. Tel.: +65 6874 4623; fax: +65 6779 1459.
E-mail address: mpeasm@nus.edu.sg (A.S. Mujumdar).

1359-4311/$ - see front matter
doi:10.1016/j.applthermaleng.2007.06.010

Nomenclature

A	porosity function
A, B	constant in Eq. (5)
C	constant
c_p	specific heat, J/kg K
g	gravitational vector, m/s^2
ΔH	latent heat of melting of PCM, J/kg
H	height of heat sink, mm
h	specific enthalpy, J/kg
h'	heat transfer coefficient, W/m^2 K
h_b	height of heat sink base, mm
h_f	height of fin, mm
k	thermal conductivity, W/m K
L	length of heat sink, mm
l_c	cavity thickness, mm
l_f	fin thickness, mm
p	pressure, Pa
q	power input, W
q''	heat flux, W/m^2
S	momentum source term
Δt	time step size, s
T	temperature, °C
t	time, s
t_s	time to steady state, s
u	velocity, m/s
W	width of heat sink, mm
x, y, z	Cartesian coordinate, m

Greek symbols

α	volume fraction
β	thermal expansion coefficient, 1/K
μ	dynamic viscosity, kg/m s
ϕ	liquid fraction of PCM
ρ	density, kg/m^3
θ	thermal resistance, °C/W
ε	constant

Subscripts

0	initial
a	ambient
air	air
c	cavity of heat sink
i	coordinate component
j	junction
ja	junction to ambient
l	liquid PCM
m	melting
n	the nth fluid
out	outlet
ref	reference
s	solid PCM
w	wall

PCM-based heat sinks can effectively store the dissipated heat from the components via phase change from solid to liquid to keep the temperature of the electronic devices below a critical temperature. Generally, the global maximum allowable temperatures of various chips range from 85 to 120 °C to prevent damage due to overheating. Furthermore, the maximum environmental temperature humans can tolerate for 1 h is 49 and 62 °C for contact with metals and non-metals, respectively, as reported by Henry Dreyfuss Associates [9]. Considering that the molten PCM needs to be re-solidified by dissipating heat to the surroundings while the electronic devices are idle, such a cooling system is applicable only for intermittent-use devices and not those in continuous operation. To achieve effective cooling it is important to ensure that the operating duration of the electronic devices does not exceed the time of full melting.

Tan and Tso [10] experimentally studied the cooling of mobile electronic devices using a heat storage unit filled with n-eicosane inside the unit and found that the effectiveness of the device depended on the amount of PCM used. Krishnan et al. [11] proposed a hybrid heat sink which combined an active plate fin heat sink with the tip immersed in a passive PCM. Akhilesh et al. [12] presented a thermal design procedure to maximize the energy storage and operating time for a composite heat sink consisting of an elemental heat sink, PCM and a highly conductive base material. Shatikian et al. [13] numerically investigated the melting of a PCM in a heat sink and generalized the results through dimensional analysis.

The objective of this work is to investigate experimentally and numerically the feasibility of using PCM-based heat sinks for application in thermal management of transient electronic devices. The heat transfer characteristics of a PCM-based heat sink placed on a quad flat package (QFP) electronic device were studied experimentally and compared with of a pure heat sink without embedded PCMs. Specified local temperature within PCMs and the die junction temperature were measured. Furthermore, a three-dimensional numerical model was proposed to compare with the experimental results.

2. Experimental setup

The experimental setup is shown schematically in Fig. 1. The heat sink was placed on top of a thermally enhanced plastic quad flat package (TEP-QFP). The QFP package (with dimension of 14 mm × 14 mm and 64 leads) was mounted on top of an FR4 printed circuit board (PCB). Fig. 1 also shows that the die was placed upside on an attached die paddle covered outside with epoxy molding compound (EMC). Heat spreader placed on top of the

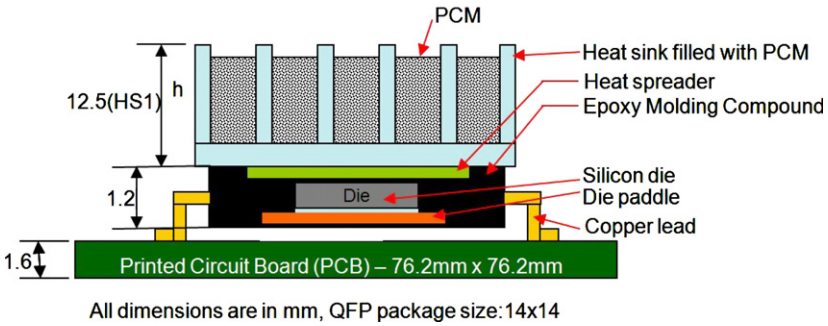

Fig. 1. Cross-sectional schematic of PCM filled heat sink with QFP package.

die within the EMC to enhance thermal performance of the QFP package. The experimental test and environment used are as described in EIA/JESD51-2 standard [14]. Before the experiment, the heat sink enclosure was slowly filled with molten PCM at a temperature of 95 °C using a hot plate. The liquid PCM was poured in the cavities and reduced the power of the hot plate continuously to allow solidification of the PCM in the absence of any entrapped air bubble. As physically displayed in Fig. 2, three types of heat sinks were tested:

- HS1: Small plate fin heat sink, 16 mm × 14 mm × 12.5 mm with 6 plate fins;
- HS2: Large plate fin heat sink, 31 mm × 31 mm × 10 mm with 10 plate fins;
- HS3: Elliptical heat sink, 30 mm × 30 mm × 18 mm with 3 × 11 row fins.

As shown in Fig. 1, the main components of this device include a PCB board, a chip module and an external heat sink embedded with a PCM. The input power range from 2 to 6 W. Paraffin wax with an average melting point of 55 °C was selected as the filling PCM. Local temperature variation with time was monitored continuously in each experiment, i.e., heat sink without PCM and heat sink with PCM. To follow the transient melting behavior of paraffin wax, six thermocouples were placed in the small plate fin heat sink (HS1). The data acquisition unit used was an Agilent 34970A Data Acquisition Unit linked to a PC. This setup enables the temperature of each thermocouple to be captured and plotted at fixed time intervals in real time. Note that the experiments were limited to a single PCM, paraffin wax, whose properties are given in Table 1.

For each case, at least three different separate runs at different times were carried out to verify reproducibility of the experimental data. The uncertainties in transient temperature recorded and power measurement at a power level of 6 W were within ±3.5% and ±0.5%, respectively. Hence the resulting uncertainty in calculated temperature and thermal resistance was within 4%.

To analyze the thermal performance of the PCM package, values of some important variables must be clarified before a detailed discussion. During the tests, the temperature of the heater should be kept below 85 °C since it is

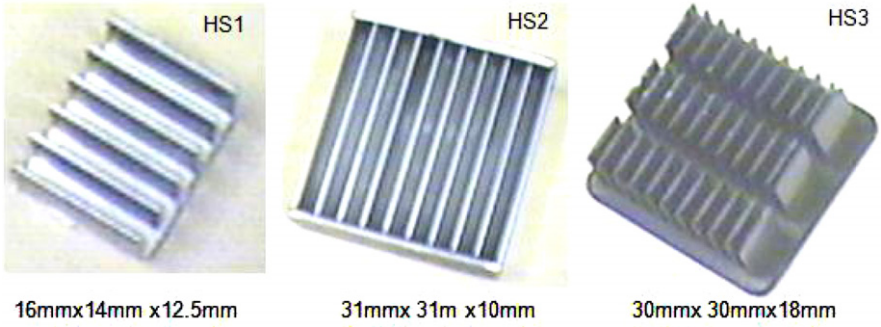

Fig. 2. Three types of heat sinks used in the experiments: HS1 (6 plate fins), HS2 (10 plate fins) and HS3 (3 × 11 row fins).

Table 1
Properties of paraffin wax, aluminum and air

	ρ (kg/m^3)	c_p (J/kg K)	k (W/m K)	T_m (°C)	ΔH (J/kg)
Paraffin wax	$\frac{800}{0.001(T-319)+1}$	2890	0.21/0.12	53–57	173,400
Aluminum	2719	871	202.4	–	–
Air	$1.2\times10^{-5}T^2-0.01134T+3.498$	1006.4	0.0242	–	–

typically the highest operating temperature permissible for most chips to ensure reliability. The performance of the CCD in digital cameras, for example, degrades above 85 °C.

3. Experimental results

The effects of the following parameters were examined in the experimental study:

- Comparison between packages with heat sink and those without heat sink.
- Comparison between packages with heat sink with PCMs and those without PCMs.
- Power levels ranging from 2, 4, to 6 W ($q'' \simeq 1$, 2, to 3 W/cm^2).
- Various designs of heat sinks: HS1, HS2 and HS3 (see Fig. 2).

First, to compare their performance with respect to the pure QFP package, packages with various types of heat sinks were examined. For a pure QFP package, Fig. 3 shows the transient temperature response of the case surface temperature and the chip temperature. It can be seen that the two temperatures initially increase with time due to the heat input (2 W in this case). After about 6–8 min, the values become constant, which means the system reaches steady state. Note that all the experimental tests were performed in a natural convection environment inside a cubical JEDEC (Joint Electron Device Engineering Council) enclosure at an ambient temperature in the range 20–23 °C. The JEDEC enclosure stipulated the use of a square cardboard enclosure of side 305 mm specified as standard for thermal testing. The variation between the package case and the chip temperature difference was measured to be 4–5 °C at 2 W, as shown in Fig. 3.

When a heat sink is attached at the top of the package, theoretically the cooling performance should be improved since the attached heat sink increases the area for convection heat transfer to the ambient. Fig. 4 displays the evolution of the junction temperature (T_j) with time for various heat sinks attached to the top of the QFP package. For input power level of 2 W, the steady peak chip temperature was 63.4 °C in the absence of an external heat sink. With the smaller heat sink (HS1) attached, the chip junction temperature decreased by 5 °C, while with the larger heat sink (HS2), a further decrease of 10 °C of the junction temperature was measured. This means that the included heat sink improves the cooling performance appreciably under the influence of natural convection. Initially, the junction temperature of HS3 is relatively higher than that of HS2. However, both HS2 and HS3 behaviors were found to be nearly same at steady state. It is reasonable since the base size of HS3 is smaller than that of HS2, although HS3 is larger in height and elliptical fin shape. These factors in HS3 might help in forced convection rather than natural convection.

The thermal resistance ($\theta_{ja} = (T_j - T_a)/q$) of the tested QFP packages at various time is shown in Fig. 5 for different heat sinks. For the case without heat sink, the thermal resistance is 21.0 °C/W at steady state. However, for the cases with heat sink, the thermal resistance is 18.1 °C/W and 15.9 °C/W for HS1 and HS2/HS3, respectively. Similar behavior of the transient junction temperature and θ_{ja} was observed from comparing Fig. 4 with Fig. 5.

Furthermore, the effect of inclusion of PCMs in the heat sink on the thermal performance of the QFP package was examined. Fig. 6 demonstrates the measured transient die junction temperature response of the package without/with

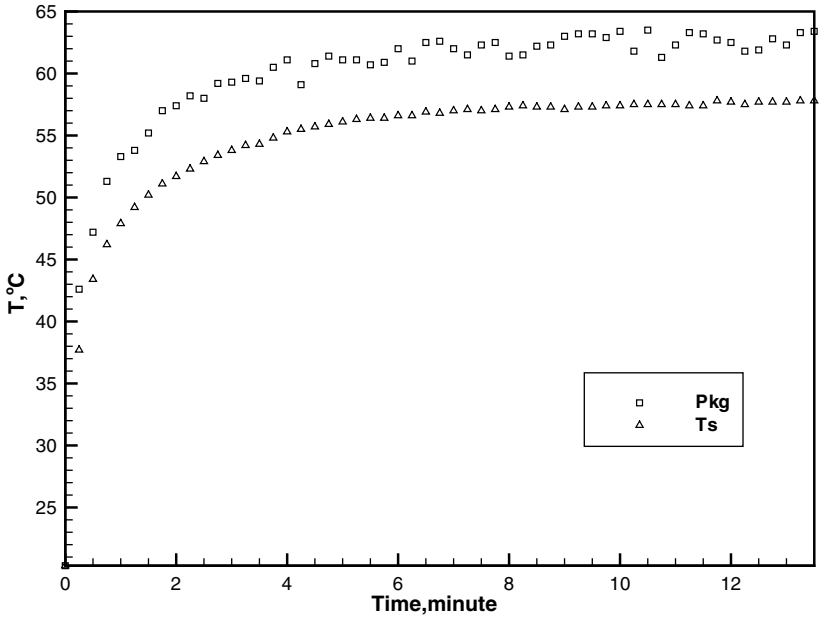

Fig. 3. Comparison between package case temperature and chip temperature for the pure QFP package case, $q = 2$ W.

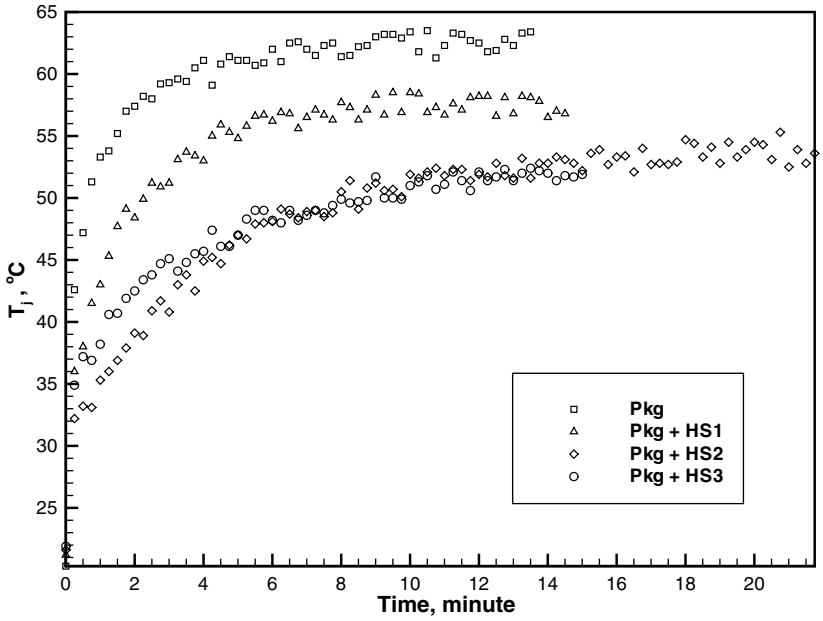

Fig. 4. Transient die junction temperature (T_j) response of QFP package for setups without PCMs, $q = 2$ W.

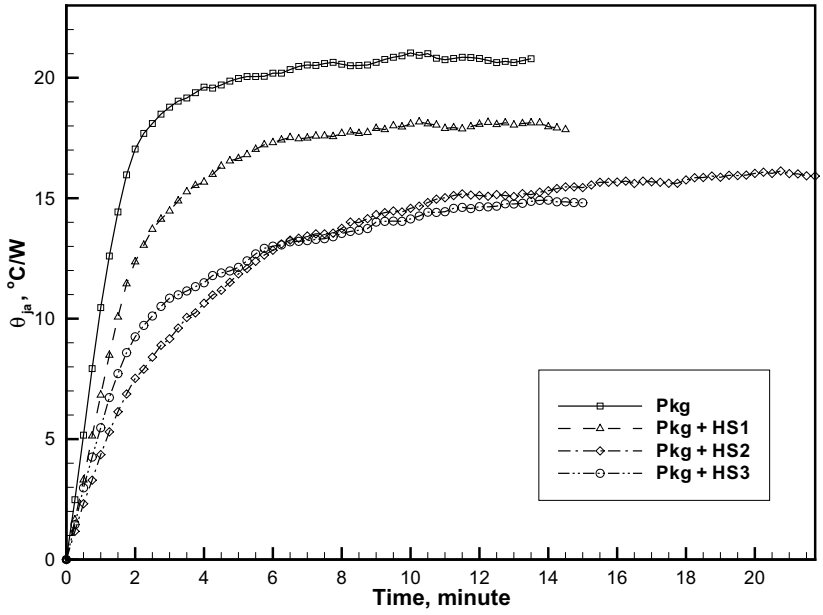

Fig. 5. Package θ_{ja} response of QFP package for packages without PCMs, $q = 2$ W.

heat sink (HS2)/with heat sink with PCM at $q = 2$ and 4 W. First, for $q = 2$ W, it was observed that with addition of heat sink, the junction temperature decreased largely. While with inclusion of PCMs in the heat sink, the junction temperature has negligible change. The small variation between package without PCMs and that with PCMs is ascribed to the low level of input power (2 W), which is too low to activate the melting of PCMs. When the power level increases from 2 W to 4 W, the effect of the presence of the PCM is seen clearly. As seen from Fig. 6, the inclusion of PCM increases the time needed to reach steady state, although the final junction temperature is same after the full melting of PCMs. The increased transient time is especially useful for transient electronic devices since they normally are switched on for a short time, followed by a usually long standby period; the re-solidification of the melted PCM occurs by loss of the heat accumulated in the molten PCM to the ambient.

The thermal resistance of the package for various test cases and power levels is shown in Fig. 7. It is found that increased power input makes heat sink with PCMs more effective for transient cooling performance. In natural convection environment, the increased chip power increases the surface temperature of the package and board, which

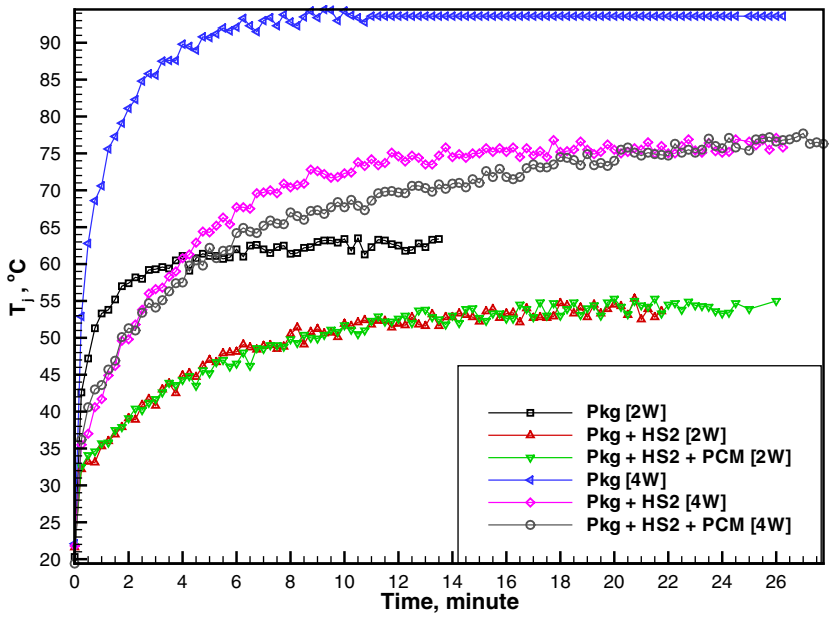

Fig. 6. Transient die junction temperature response of QFP package for various cases at $q = 2$, 4 W.

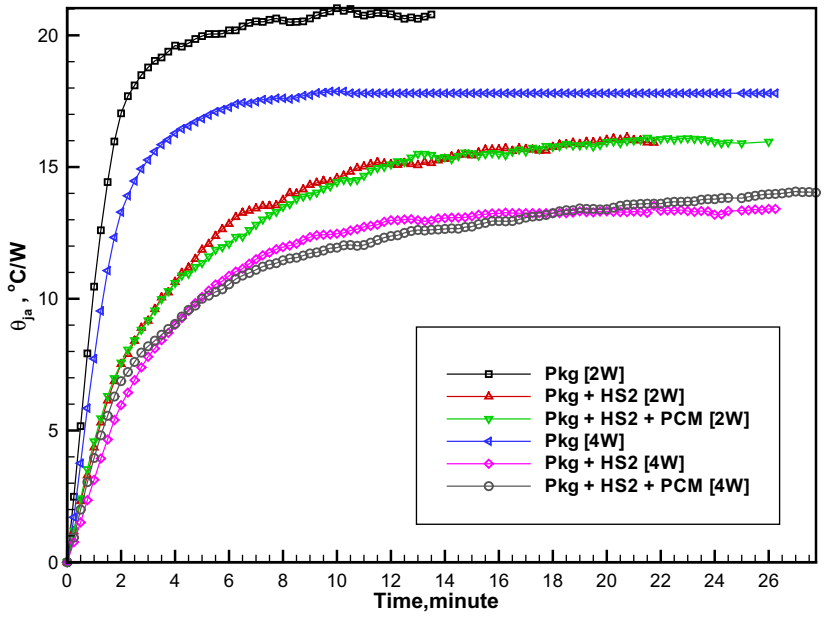

Fig. 7. Package θ_{ja} response of QFP package for various cases at $q = 2$, 4 W.

in turn enhances buoyancy effect as well as additional radiation heat loss. Hence, the overall thermal resistance of the package with higher power level is relatively lower than that with lower power input. Note that data only for HS2 are analyzed here. Similar trends were observed for the other two types of heat sinks.

For 4 W power input, Fig. 8 shows the evolution of the temperature difference between the junction temperature (T_j) and the ambient temperature (T_a) with time for three cases: pure package (no heat sink), package with HS2, package with a hybrid heat sink viz. HS2 and PCM. It should be noted that for all cases, steady state could be reached within a reasonable time. As seen from this figure, for pure QFP package without heat sink, the time (t_s) to reach the final steady state is about 5.5 min, while the steady temperature difference ($T_j - T_a$) is about 71 °C. With heat sink (HS2), t_s increased from 5.5 to 11 min, while $T_j - T_a$ decreased from 71 to 53 °C. Furthermore, with the hybrid heat sink filled with PCM, the final $T_j - T_a$ remained the same as that for heat sink without PCM, but t_s increased approximately to 41 min. Since high temperature is not desired in electronic cooling application, to keep the system at a lower temperature for longer time is desirable. It is clear that inclusion of PCMs increases

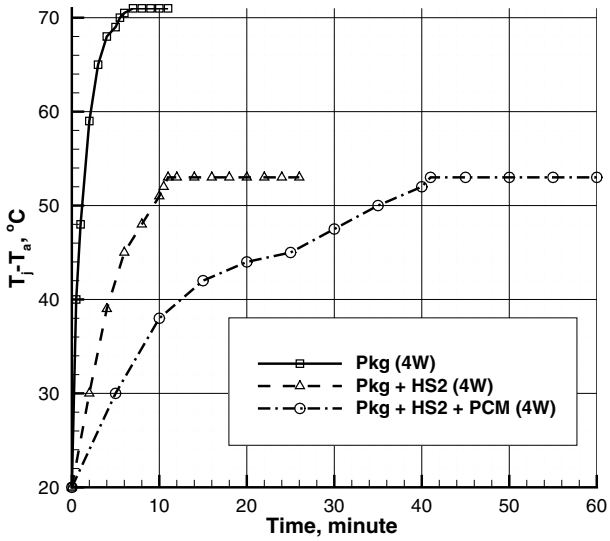

Fig. 8. Evolution of $T_j - T_a$ with time for package with HS2 at 4 W.

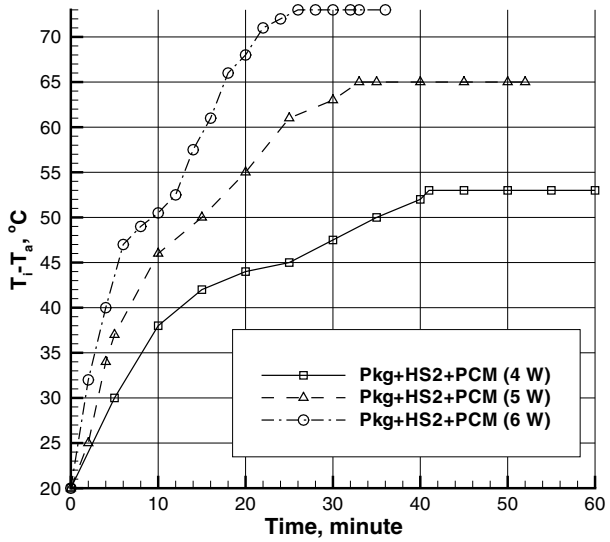

Fig. 9. Evolution of $T_j - T_a$ with time for HS2 at different power levels.

the time t_s and thus allows operation of intermittently used devices over longer periods of time. Similar trends were found for the other two heat sinks.

Now it is useful to compare the effect of various power levels. Fig. 9 displays the evolution of $T_j - T_a$ with time for HS2 at various power inputs. It is concluded from this figure that increased power input results in decrease of t_s and increase of $T_j - T_a$ at final steady state. For example, at power levels of 4, 5 and 6 W, the corresponding steady $T_j - T_a$ was found to be 53, 65 and 73 °C, while the t_s values were 41, 33 and 26 min, respectively.

The smaller heat sink (HS1) was used to observe the PCM temperature with time. Fig. 10 shows the internal PCM melting temperature validation with time of one of the thermocouples at various input power in one specified middle location. It should be noted that the PCM did not melt when the input power level is lower than 4 W. Hence, melting point of 55 °C was too high for heat recovery for $q < 4$ W.

4. Numerical model

A schematic diagram of three-dimensional physical model is shown in Fig. 11. Considering the symmetry of the geometry, only one quarter of the physical model is included for computation. The 3D numerical model was developed to compare the trends observed in the experimental results. It represents the small heat sink (HS1) used in the experimental program. The heat sink is made of aluminum and the cavities hold the PCM (paraffin wax). A uniform heat flux, q'', is applied on the bottom surface of the heat sink unit ($L \times W \times H = 16 \times 14 \times 12.5$ mm^3). Six aluminum walls of 1.21 mm thickness (l_f) separate the heat sink into five cavities of equal width, $l_c = 2$ mm and the thickness of the bottom base (h_b) is 1.5 mm. The PCMs are filled in the cavities to a height of 11 mm (h_f). The top faces of all the cavities are enclosed to prevent leakage of the PCM during melting at various orientations. To allow for the expansion of the PCM during melting, the PCM is not filled to the brim in the cavities; the remaining volume is occupied by air. Thus, the air volume will be compressed during melting of PCMs as the liquid expands. It is assumed that heat is transferred between the PCM and the base, the fins, the end walls as well as the entrapped air. Following the suggestion of Shatikian et al. [13], a relatively small PCM-based heat sink system is chosen since such heat sinks are currently used in cooling applications for electronic components.

To describe the PCM–air system with a moving internal interface but without inter-penetration of the two fluids, the volume-of-fluid (VOF) model has been used successfully [15]. In the VOF model, if the nth fluid's volume fraction in the computational cell is denoted as α_n, then the following three conditions are possible: if $\alpha_n = 0$ the cell is empty of the nth fluid; if $\alpha_n = 1$ the cell is full of the nth fluid; and if $0 < \alpha_n < 1$ the cell contains the interface between the nth fluid and one or more other fluids. Thus, the variables and properties in any given cell are either purely representative of one of the media, or representative of a mixture of the media, depending upon their volume fraction values. Furthermore, considering compressibility of the air during melting, a compressible model was used.

Accordingly, the governing equations which model the hybrid system [16] are

$$\text{Continuity} \quad \frac{\partial \alpha_n}{\partial t} + u_i \frac{\partial \alpha_n}{\partial x_i} = 0 \tag{1}$$

$$\text{Momentum} \quad \frac{\partial}{\partial t}(\rho_n u_i) + \frac{\partial}{\partial x_j}(\rho_n u_j u_i) = -\frac{\partial p}{\partial x_i} + \frac{\partial}{\partial x_j}\left[\mu\left(\frac{\partial u_i}{\partial x_j} + \frac{\partial u_j}{\partial x_i} - \frac{2}{3}\delta_{ij}\frac{\partial u_l}{\partial x_l}\right)\right] + \rho_n g_i + S_{n,i} \tag{2}$$

$$\text{Energy} \quad \frac{\partial}{\partial t}(\rho_n h) + \frac{\partial}{\partial x_i}(\rho_n u_i h) = \frac{\partial}{\partial x_i}\left(k_n \frac{\partial T}{\partial x_i}\right) \tag{3}$$

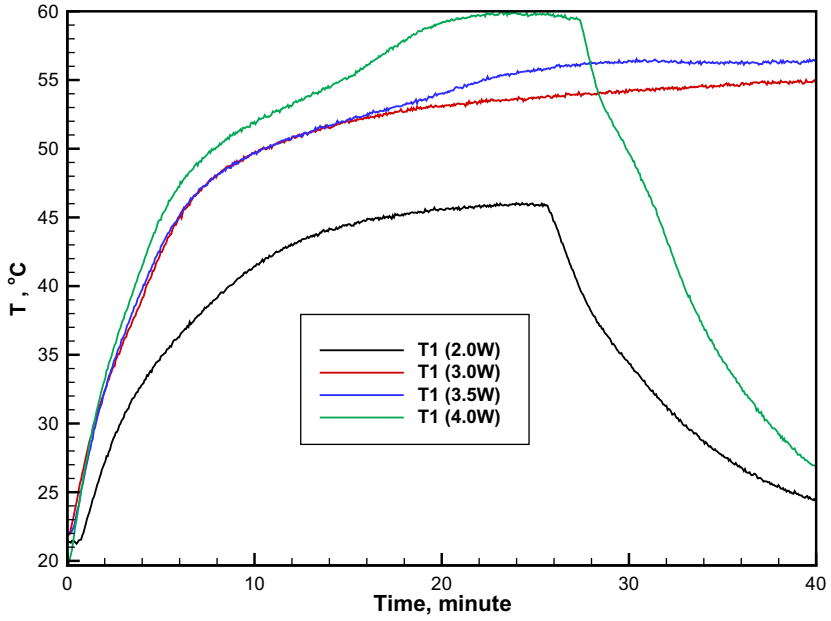

Fig. 10. PCM melting temperature response with time for different power levels.

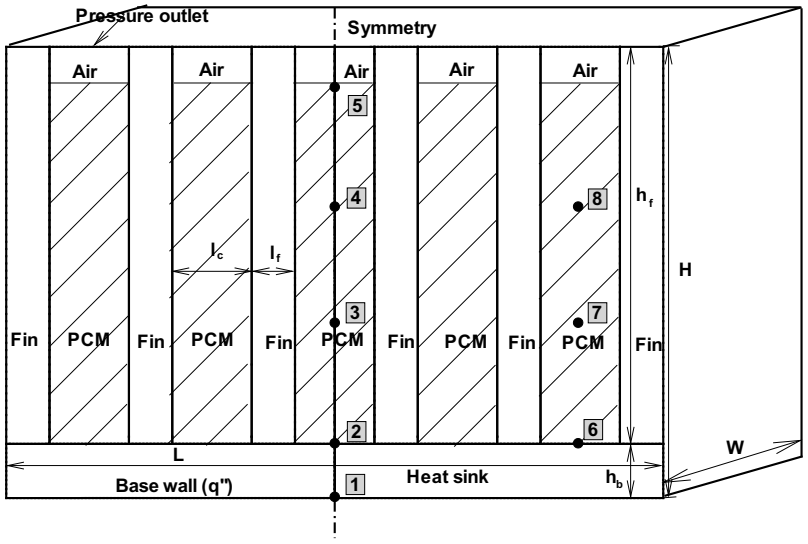

Fig. 11. Three-dimensional physical model.

where α_n is the nth fluid's volume fraction in the computational cell, ρ_n, k_n and μ_n are the density, thermal conductivity and dynamic viscosity of the nth fluid, respectively. $S_{n,i}$ is the momentum source term, which is equal to zero for air phase, but $S_i = -A(\phi)u_i$ for PCM phase. Here $A(\phi)$ is the "porosity function" defined by Brent et al. [17] to make the momentum equation mimic Carman–Kozeny equations for the flow in porous media: $A(\phi) = C(1-\phi^2)/(\phi^3+\varepsilon)$ with $\varepsilon = 0.001$ and $C = 10^5$ used here. Also, u_i is the velocity component, x_i is a Cartesian coordinate and h is the specific enthalpy defined as, $h = h_{\text{ref}} + \int_{T_{\text{ref}}}^{T} c_p \, \mathrm{d}T$ and the enthalpy change due to the phase change is $\phi\Delta H$, at reference temperature T_{ref}, c_p is the specific heat, ΔH is the latent heat of the PCM and ϕ is the liquid fraction during the phase change which occurs over a range of temperatures $T_{\text{solidus}} < T < T_{\text{liquidus}}$.

Since the proposed PCM-based heat sink problem is time-dependent, initial and boundary conditions must be set appropriately before the calculation starts. With reference to the origin indicated in Fig. 11

$$\text{I.C.: } t \leqslant 0, \quad T = T_0 \quad \text{for } -\frac{L}{2} \leqslant x \leqslant \frac{L}{2}; \quad -h_{\text{b}} \leqslant y \leqslant h_{\text{f}}$$

$$\text{B.C.: } t > 0, \quad (y = -h_{\text{b}}) = T_{\text{w}}(x)$$

$$h'\left(x = \pm\frac{L}{2}\right) = h'_{\text{a}}$$

$$\text{Air top:} \quad P_{\text{air,out}}(y = h_{\text{f}}) = P_{\text{a}}$$

$$\text{Fin top:} \quad h'(y = h_{\text{f}}) = h'_{\text{a}}$$

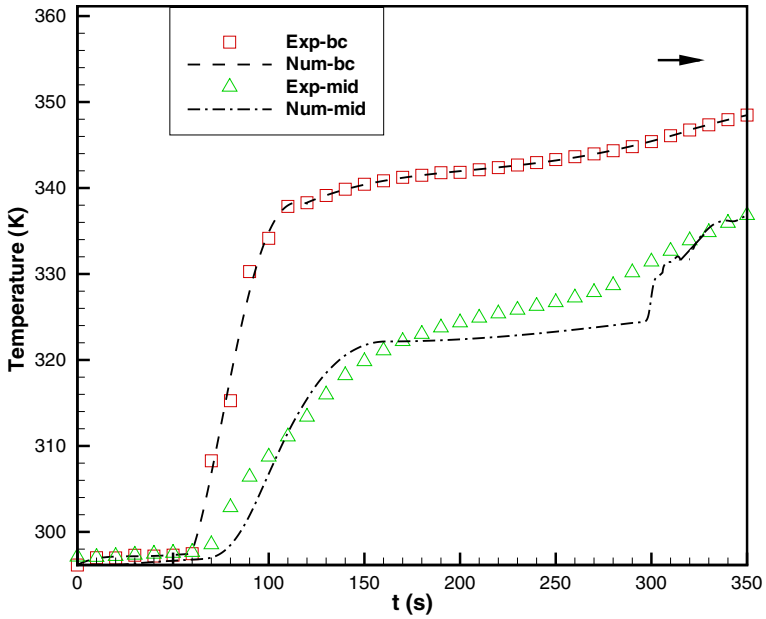

Fig. 12. Evolution of specified local temperature at bottom wall and middle point with time for 3D simulation of HS1 at 4 W.

where $T_w(x)$ is the boundary temperature on the bottom surface of the heat sink measured in experiment, although the constant power supply (q) was set in experiment.

As shown in Table 1, for the air phase, density depends on temperature. For aluminum, constant thermophysical properties are specified. For the PCM phase, considering computational continuity during phase change, its density can be expressed as

$$\rho = \frac{\rho_l}{\beta(T - T_m) + 1} \tag{4}$$

Here $\beta = 0.001$ as suggested by Humphries and Griggs [18].

The dynamic viscosity of liquid PCM is given by

$$\mu = 0.001 \times \exp(A + B/T) \tag{5}$$

where $A = -4.25$ and $B = 1790$ following Reid et al. [19].

The numerical solution of the governing equations was carried out using the Fluent 6.2 software [16]. The PISO (Pressure Implicit with Splitting of Operator) algorithm was selected for the pressure–velocity coupling. The computational grids were in the range of 150,000 for the 3D model following grid-independence test. Furthermore, after a careful examination of the preliminary calculations, the time step size in the simulations had to be set as small as $\Delta t = 0.01$ s. Convergence was also checked at each time step, with the convergence criterion of 10^{-4} for the velocity components and 10^{-7} for energy.

5. Numerical results

The local temperature at the middle position ($x = 3.4$, $y = 7$, $z = 0$ mm) in the heat sink (HS1) was selected to monitor the temperature variation with time. The comparison of the specified temperature between the experiment and simulation is shown in Fig. 12. It is noted that the numerically input boundary temperature at the bottom surface of the heat sink was simulated using a multi-stage polynomial formula. First, both the experimental and numerical temperature curves show three distinct regions: pre-melting, melting and post-melting. In the first stage, the PCM is heated by pure conduction. Hence the curve shows nearly a linear relation between temperature and time. Once the local temperature reaches the melting point, the PCM starts to melt and maintains the temperature at its range of melting points. In the last stage, due to combination of conduction and free convection of the melted PCM, the temperature gradient is higher than that in the second region.

Furthermore, Fig. 12 displays the good agreement observed between the experimental data and numerical results. The small discrepancy may attributed to the inaccuracies in specifying the true boundary conditions. For example, the heat transfer coefficient between the walls and the ambient was assumed to be constant in the simulation. However, it can be slightly different in the experiment. Hence, the discrepancy is expected to be minimal for an improved model with more precise boundary conditions and material properties.

The time evolution of the liquid fraction contours for the 3D HS1 at a power level of 4 W is shown in Fig. 13. Note that the red color denotes liquid phase and the blue color denotes solid phase.[1] It can be observed from the figure that the evolution of the liquid fraction of the PCM starts from all the walls due to heat conduction in the aluminum fins. It is interesting to observe that the trapped air improves the heat transfer rate to the PCM in contact with

[1] For interpretation of color in Fig. 13, the reader is referred to the web version of this article.

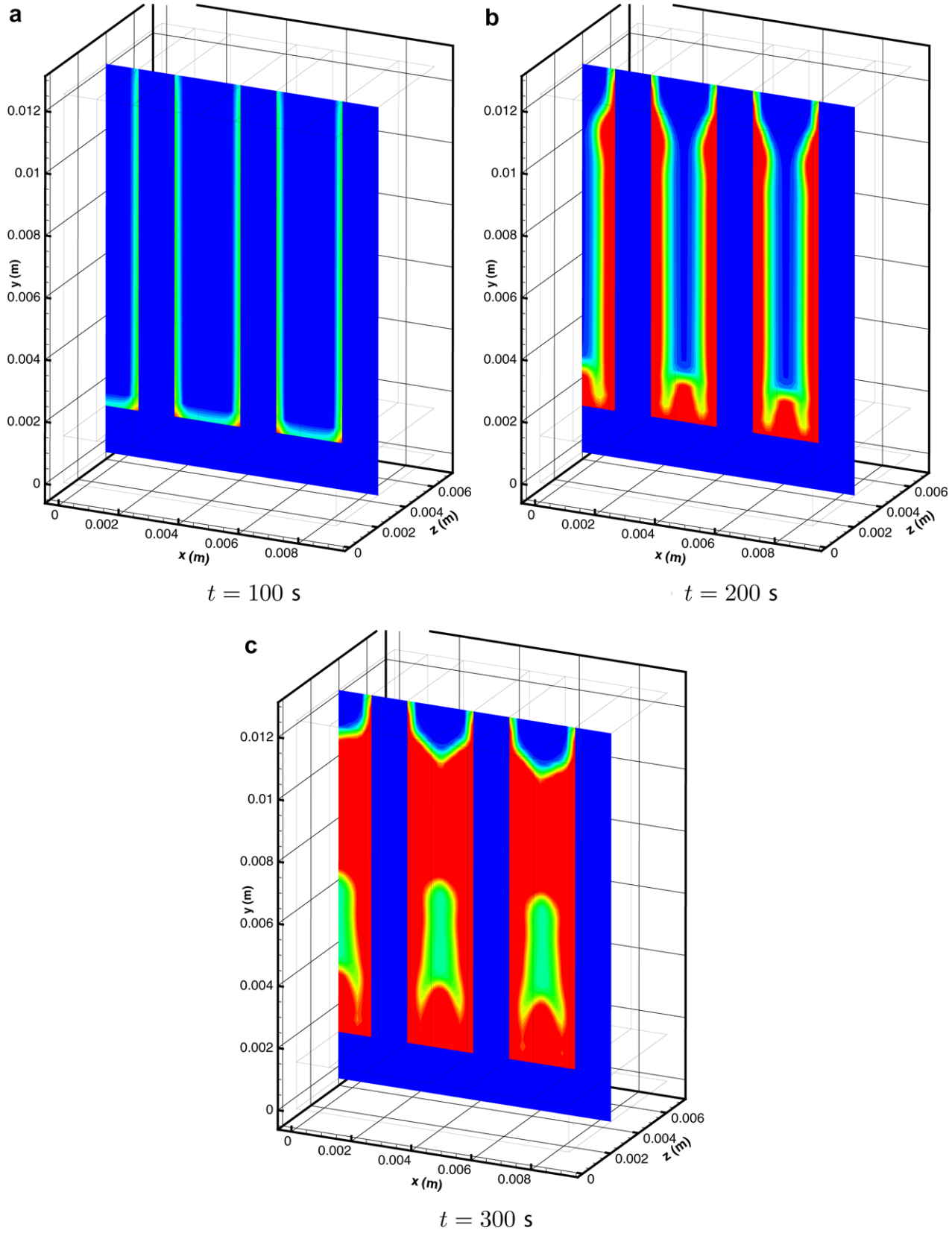

Fig. 13. Liquid fraction contours for various time for 3D simulation of HS1 at 4 W.

it. When the air temperature reaches the PCM melting point, the PCM near the top side begins to melt and causes the temperature to increase from the top side and results in melting of PCM in contact with the air. It also can be observed from this figure that during melting of the PCM, its volume expands and squeezes trapped the air.

Finally, a curved interface between liquid and air is formed, as shown in Fig. 13.

6. Conclusions

A well designed PCM-based heat sink for various power levels was investigated experimentally and numerically. Results show that the inclusion of PCM in the cavities of the heat sinks will increase the cooling performance as compared to the cases without involved PCM when the input power level is relatively high ($q > 2$ W in this study). Furthermore, the numerical results of a three-dimensional simulation show good agreement with the experimental data. Such designs should have great potential in the transient electronic cooling applications.

References

[1] Z.X. Gong, A.S. Mujumdar, A new solar receiver thermal store for space-based activities using multiple composite phase change materials, ASME Journal of Solar Energy Engineering 117 (1995) 215–220.
[2] Z.X. Gong, A.S. Mujumdar, Cyclic heat transfer in a novel storage unit of multiple phase change materials, Applied Thermal Engineering 16 (10) (1996) 807–815.
[3] Z.X. Gong, A.S. Mujumdar, Enhancement of energy charge-discharge rates in composite slabs of different phase change materials, International Journal of Heat and Mass Transfer 39 (4) (1996) 725–733.
[4] Z.X. Gong, A.S. Mujumdar, Thermodynamic optimization of the thermal process in energy storage using multiple phase change materials, Applied Thermal Engineering 17 (11) (1997) 1067–1083.
[5] R. Kandasamy, X.-Q. Wang, A.S. Mujumdar, Application of phase change materials in thermal management of electronics, Applied Thermal Engineering, in press, doi:10.1016/j.applthermaleng.2006.12.013.
[6] X.-Q. Wang, C. Yap, A.S. Mujumdar, Cyclic melting and freezing heat transfer using paired phase change materials, in: B. Thorat, S. Devahastin, G. Chen (Eds.), Topics Heat and Mass Transfer, 2004.
[7] R. Velraj, R.V. Seeniraj, B. Hafner, C. Faber, K. Schwarzer, Heat transfer enhancement in a latent heat storage system, Solar Energy 65 (3) (1999) 171–180.
[8] B. Zalba, J.M. Marin, L.F. Cabeza, H. Mehlin, Free-cooling of building with phase change materials, International Journal of Refrigeration 27 (2004) 839–849.
[9] A.R. Tilley, H.D. Associates, The Measure of Man and Women, Human Factors in Design, revised edition Edition., Whitney Library of Design, Watson-Guptill Publications, 2001.
[10] F. Tan, C. Tso, Cooling of mobile electronic devices using phase change materials, Applied Thermal Engineering 24 (2004) 159–169.
[11] S. Krishnan, S. Garimella, S. Kang, A novel hybrid heat sink using phase change materials for transient thermal management of electronics, in: Proceedings of 2004 Inter Society Conference on Thermal Phenomena (ITHER M04), 2004, pp. 310–318.
[12] R. Akhilesh, A. Narasimhan, C. Balaji, Method to improve geometry for heat transfer enhancement in PCM composite heat sinks, International Journal of Heat and Mass Transfer 48 (13) (2005) 2759–2770.
[13] V. Shatikian, G. Ziskind, R. Letan, Numerical investigation of a PCM-based heat sink with internal fins, International Journal of Heat and Mass Transfer 48 (17) (2005) 3689–3706.
[14] EIA/JESD51-2, Integrated circuits thermal test method environment conditions – natural convection (still air).
[15] C. Hirt, B. Nichols, Volume of fluid (VOF) method for the dynamics of free boundaries, Journal of Computational Physics 39 (1981) 201.
[16] http://www.fluent.com.
[17] A. Brent, V. Voller, K. Reid, Enthalpy-porosity technique for modeling convection–diffusion phase change: application to the melting of a pure metal, Numerical Heat Transfer, Part A 13 (1988) 297–318.
[18] W. Humphries, E. Griggs, A design handbook for phase change thermal control and energy storage devices, Tech. rep., 1074NASA Scientific and Technical Information Office, 1977.
[19] R. Reid, J. Prausnitz, B. Poling, The Properties of Gases and Liquids, McGraw-Hill, New York, 1987.